A Dual-Vector Modulated Model Predictive Control Method for Voltage Source Inverters with a New Duty Cycle Calculation Method

Lingzhi Cao [1], Yanyan Li [1],*, Xiaoying Li [2], Leilei Guo [1], Nan Jin [1] and Hong Cao [2]

[1] School of Electrical and Information Engineering, Zhengzhou University of Light Industry, Zhengzhou 450002, China; caolingzhi@zzuli.edu.cn (L.C.); 2016guoleilei@zzuli.edu.cn (L.G.); jinnan@zzuli.edu.cn (N.J.)

[2] Senyuan Electric Co., Ltd., Changge 461500, China; xacyjd@126.com (X.L.); caoh@hnsyec.com (H.C.)

* Correspondence: 2017069@zzuli.edu.cn; Tel.: +86-1583-811-4911

Abstract: Recently, model predictive control (MPC) methods have been widely used to achieve the control of two-level voltage source inverters due to their superiorities. However, only one of the eight basic voltage vectors is applied in every control cycle in the conventional MPC system, resulting in large current ripples and distortions. To address this issue, a dual-vector modulated MPC method is presented, where two voltage vectors are selected and utilized to control the voltage source inverter in every control cycle. The duty cycle of each voltage vector is figured out according to the hypothesis that it is inversely proportional to the square root of its corresponding cost function value, which is the first contribution of this paper. The effectiveness of this assumption is verified for the first time by a detailed theoretical analysis shown in this paper based on the geometrical relationship of the voltage vectors, which is another contribution of this paper. Moreover, further theoretical analysis shows that the proposed dual-vector modulated MPC method can also be extended to control other types of inverters, such as three-phase four-switch inverters. Detailed experimental results validate the effectiveness of the presented strategy.

Keywords: model predictive control; dual-vector; duty cycle; theoretical analysis

1. Introduction

Due to the advantages of two-level voltage source inverters, they have received more and more attention in the field of renewable energy generation systems, including photovoltaic systems and energy storage systems, among others. Recently, the control methods of two-level voltage source inverters have been widely studied to achieve smooth and flexible energy conversion [1–5]. As is known, vector control is widely used to control two-level voltage source inverters in renewable energy generation systems as it can achieve power decoupling control. Nevertheless, proportional and integral controller and pulse width modulation modules are needed, which makes the control system hard to debug and prolongs the development cycle of the control system. Another control method, i.e., direct power control, has also been studied to control two-level voltage source inverters. Compared to vector control, proportional and integral controller and pulse width modulation modules are removed. However, as the switching frequency is unfixed and the optimal voltage vector is selected based on an offline switch table, its power control precision is relatively low.

As a simple but effective control method, model predictive control (MPC) has received much more attention in the field of the optimal control of two-level voltage source inverters lately.

An MPC strategy was designed to control the current of two-level voltage source inverters in [6] in 2007. From then on, many researchers began to study new MPC strategies to reduce the computational

time [7,8], to lower the switching frequency [9,10], to suppress the common-mode voltage [11,12], to decrease the current ripples [13–29], or to minimize the power ripples [30–32].

In [7,8], according to the deadbeat control principle, voltage-based cost functions are designed to replace the conventional current-based cost function. Thus, the calculation burden is reduced significantly. In [9,10], the concept of multistep MPC is studied and evaluated, which can reduce the switching frequency obviously, making it very suitable for large power converters. In [11,12], common-mode voltage suppression methods are studied using an MPC strategy. Thus, the negative effects of the common-mode voltage are reduced.

Additionally, as a flexible control method, MPC strategies are also studied in [13–29] to reduce the current ripples by using more voltage vectors instead of only one in every control cycle. In [13–15], dual-vector MPC strategies are studied. Compared to the conventional single-vector MPC, the control precision is improved as more voltage vectors are utilized in every control cycle. Moreover, in [16–21], three voltage vectors are chosen per control cycle to further enhance the control performance, and better results are obtained. In these methods in [13–21], the duty cycles of each voltage vector are figured out according to the deadbeat control theory. Although duty cycles can be calculated accurately theoretically, the actual calculated duty cycle may be smaller than zero or larger than one, which reduces the control performance to a certain extent.

Alternately, there is another way to determine the duty cycles, which is named modulated MPC [22–29]. In this type of method, the duty cycle of each voltage vector is deduced by assuming that it is inversely proportional to its cost function value. As it is simple but effective, many researchers have studied modulated MPC to control the cascaded H-bridge converter [22], the multilevel solid-state transformer [23], the direct and indirect matrix converter [24,25], the shunt active filter [26], the brushless doubly fed induction machine [27], the two-level three-phase inverter [28,29], and so on. However, although it is shown in [22–29] that the modulated MPC method can achieve current control, up to now, there still lacks a solid theoretical support for this kind of method, which hinders its popularization and application.

Additionally, to minimize the power ripples of the converters, modified MPC strategies have also been studied in [26,30–32]. However, there are still few papers to study the optimal modulated model predictive direct power control methods as well as the theoretical analysis for power converters.

To fill this gap, a novelty dual-vector modulated MPC strategy is presented for two-level voltage source inverters with a new duty cycle calculation method as well as a detailed theoretical analysis. First, twelve hybrid voltage vectors are constructed according to the eight basic voltage vectors of the two-level voltage source inverter. Next, to decrease the computation amount, the reference voltage is deduced based on the reference current, and a cost function based on the voltage error is designed. Then, only three hybrid voltage vectors are required to be evaluated online per control period based on the information of the reference voltage. Finally, the optimal voltage vector combination is selected.

The main contributions of this paper lie in three aspects.

The first one is that a new duty cycle calculation method of each voltage vector is proposed in this paper according to the hypothesis that it is inversely proportional to the square root of its cost function value.

The next one is that, based on a detailed theoretical analysis, the validity of the presented dual-vector modulated MPC strategy with the new duty cycle calculation method is proved based on the geometrical relationship of the voltage vectors, which is also verified by experimental results.

The third one is that the proposed dual-vector modulated MPC strategy can also be applied to control other types of inverters, such as three-phase four-switch inverters, whose effectiveness is also proved by the geometrical relationship of the voltage vectors as well as the experimental results.

2. Conventional MPC Strategy

Figure 1 depicts the topology of two-level voltage source inverters. As is known, there are eight voltage vectors for two-level voltage source inverters, including $u_0(000)$, $u_1(100)$, $u_2(110)$, $u_3(010)$, $u_4(011)$, $u_5(001)$, $u_6(101)$, and $u_7(111)$, which are shown in Figure 2.
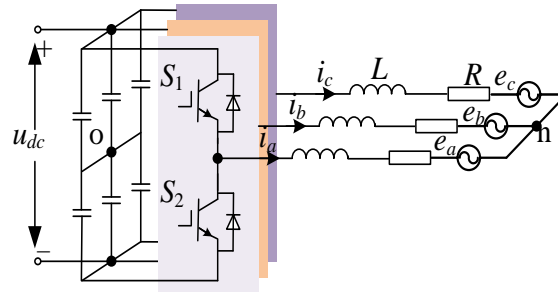
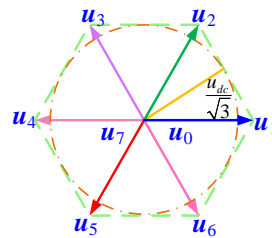**Figure 1.** Topology of two-level voltage source inverters.

Figure 2. The eight basic voltage vectors.

Typically, (1) shows the mathematical equation of two-level voltage source inverters on the α-β reference.

$$L\frac{d}{dt}\begin{bmatrix} i_\alpha \\ i_\beta \end{bmatrix} = \begin{bmatrix} u_\alpha \\ u_\beta \end{bmatrix} - R\begin{bmatrix} i_\alpha \\ i_\beta \end{bmatrix} - \begin{bmatrix} e_\alpha \\ e_\beta \end{bmatrix} \tag{1}$$

where u_α, u_β and i_α, i_β are the output AC voltages and currents, respectively, and e_α and e_β are the back electromotive forces (EMFs). L stands for the filter inductance with R denoting the parasitic resistance on it.

If the sample and control cycle is T, based on the Euler's discretization formula, it can be calculated that

$$\frac{L}{T}\begin{bmatrix} i_\alpha(k+1) - i_\alpha(k) \\ i_\beta(k+1) - i_\beta(k) \end{bmatrix} = \begin{bmatrix} u_\alpha(k) \\ u_\beta(k) \end{bmatrix} - R\begin{bmatrix} i_\alpha(k) \\ i_\beta(k) \end{bmatrix} - \begin{bmatrix} e_\alpha(k) \\ e_\beta(k) \end{bmatrix} \tag{2}$$

Based on (2), as well as the sampled current $i_\alpha(k)$ and $i_\beta(k)$ at the kth instant, the current $i_\alpha(k+1)$ and $i_\beta(k+1)$ at the next control cycle can be calculated, as depicted in (3).

$$\begin{bmatrix} i_\alpha(k+1) \\ i_\beta(k+1) \end{bmatrix} = \left(1 - \frac{RT}{L}\right)\begin{bmatrix} i_\alpha(k) \\ i_\beta(k) \end{bmatrix} + \frac{T}{L}\begin{bmatrix} u_\alpha(k) - e_\alpha(k) \\ u_\beta(k) - e_\beta(k) \end{bmatrix} \tag{3}$$

As there is an inherent one-step delay in the MPC system, to reduce its influences, it can be compensated by using the optimal voltage vector selected in the last control period to predict the current $i_\alpha(k+1)$ and $i_\beta(k+1)$ firstly. Next, the eight basic voltage vectors $u_{k+1} = [u_\alpha(k+1), u_\beta(k+1)]^T$ can be further utilized to calculate the current $i_\alpha(k+2)$ and $i_\beta(k+2)$ based on (4).

$$\begin{bmatrix} i_\alpha(k+2) \\ i_\beta(k+2) \end{bmatrix} = \left(1 - \frac{RT}{L}\right)\begin{bmatrix} i_\alpha(k+1) \\ i_\beta(k+1) \end{bmatrix} + \frac{T}{L}\begin{bmatrix} u_\alpha(k+1) - e_\alpha(k+1) \\ u_\beta(k+1) - e_\beta(k+1) \end{bmatrix} \tag{4}$$

Finally, by evaluating the prediction errors of all the eight basic voltage vectors using the cost function defined in (5), an optimal voltage vector can be chosen and utilized to control the inverter during the next control cycle.

$$g = (i_{\alpha\text{ref}} - i_\alpha(k+2))^2 + (i_{\beta\text{ref}} - i_\beta(k+2))^2 \tag{5}$$

where $i_{\alpha\text{ref}}$ and $i_{\beta\text{ref}}$ are the reference currents.

As only one voltage vector is utilized in every control cycle in the above conventional MPC strategy, the current total harmonic distortion (THD) is quite large.

Aiming to solve this problem, a dual-vector modulated MPC strategy is presented in this paper by using two voltage vectors in every control cycle. Detailed theoretical analysis is carried out to verify the validity of the presented dual-vector modulated MPC strategy. Comparative experimental results also verified its effectiveness.

3. Dual-Vector Modulated MPC Strategy

According to [7,8], to simplify the MPC strategy, a cost function based on the reference voltage is defined in this paper.

First, the reference voltage is deduced according to the deadbeat control theory, which is shown in (6).

$$\begin{bmatrix} u_{\alpha\text{ref}} \\ u_{\beta\text{ref}} \end{bmatrix} = R \begin{bmatrix} i_\alpha(k+1) \\ i_\beta(k+1) \end{bmatrix} + \begin{bmatrix} e_\alpha(k+1) \\ e_\beta(k+1) \end{bmatrix} + \frac{L}{T} \left(\begin{bmatrix} i_{\alpha ref} \\ i_{\beta ref} \end{bmatrix} - \begin{bmatrix} i_\alpha(k+1) \\ i_\beta(k+1) \end{bmatrix} \right) \tag{6}$$

where $u_{\alpha\text{ref}}$ and $u_{\beta\text{ref}}$ are the reference voltages.

To limit the voltage within the linear modulation region, if $u_m = \sqrt{u_{\alpha\text{ref}}^2 + u_{\beta\text{ref}}^2} > u_{dc} / \sqrt{3}$, $u_{\alpha\text{ref}}$ and $u_{\beta\text{ref}}$ are calculated based on (7).

$$\begin{cases} u_{\alpha\text{ref}} = \frac{u_{\alpha\text{ref}}}{u_m} \frac{u_{dc}}{\sqrt{3}} \\ u_{\beta\text{ref}} = \frac{u_{\beta\text{ref}}}{u_m} \frac{u_{dc}}{\sqrt{3}} \end{cases} \tag{7}$$

Then, a voltage-based cost function is defined as

$$G = (u_{\alpha\text{ref}} - u_\alpha(k))^2 + (u_{\beta\text{ref}} - u_\beta(k))^2 \tag{8}$$

Through using this voltage-based cost function, the calculation burden can be reduced as the prediction of the current for many times in each control cycle is not required any more.

To select and apply two voltage vectors per control period, twelve hybrid voltage vectors are constructed according to the eight basic voltage vectors of the two-level voltage source inverter. They are $u_{s1}(u_0, u_1)$, $u_{s2}(u_1, u_2)$, $u_{s3}(u_7, u_2)$, $u_{s4}(u_2, u_3)$, $u_{s5}(u_0, u_3)$, $u_{s6}(u_3, u_4)$, $u_{s7}(u_7, u_4)$, $u_{s8}(u_4, u_5)$, $u_{s9}(u_0, u_5)$, $u_{s10}(u_5, u_6)$, $u_{s11}(u_7, u_6)$, and $u_{s12}(u_6, u_1)$, respectively, which are illustrated in Figure 3.
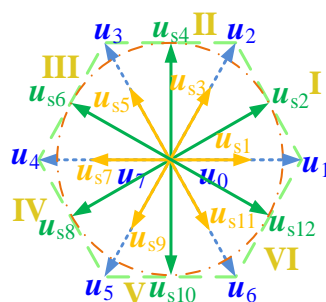

Figure 3. Hybrid voltage vectors.

The relationship between the twelve constructed hybrid voltage vectors and the basic voltage vectors is depicted in (9).

$$\boldsymbol{u}_{si} = d_{i,uj}\boldsymbol{u}_j + d_{i,uk}\boldsymbol{u}_k \tag{9}$$

where $d_{i,uj} + d_{i,uk} = 1$, $d_{i,uj}$ is the duty cycle of $\boldsymbol{u}_j$ and $d_{i,uk}$ is the duty cycle of $\boldsymbol{u}_k$.

For example, as $\boldsymbol{u}_{s1}$ is combined by $\boldsymbol{u}_0$ and $\boldsymbol{u}_1$, their relationship can be expressed as

$$\boldsymbol{u}_{s1} = d_{1,u0}\boldsymbol{u}_0 + d_{1,u1}\boldsymbol{u}_1 \tag{10}$$

To calculate the values of the twelve constructed hybrid voltage vectors, the duty cycles of the basic voltage vectors should be calculated first. Different from the methods in [22–29], which lack theoretical support, here a new duty cycle calculation method is proposed by assuming that it is inversely proportional to the square root of its cost function value, as shown in (11), where m is a positive coefficient. In Section 4, the effectiveness of this proposed hypothesis is verified in detail by a particular theoretical analysis.

$$d_i = \frac{m}{\sqrt{G_i}} \tag{11}$$

Based on (9) and (11), the duty cycles of the basic voltage vectors are deduced. For instance, the duty cycles of $\boldsymbol{u}_0$ and $\boldsymbol{u}_1$ that construct $\boldsymbol{u}_{s1}$ can be calculated based on (12).

$$\begin{cases} d_{1,u0} = \dfrac{\sqrt{G_1}}{\sqrt{G_0} + \sqrt{G_1}} \\ d_{1,u1} = \dfrac{\sqrt{G_0}}{\sqrt{G_0} + \sqrt{G_1}} \end{cases} \tag{12}$$

where G_0 and G_1 are the values of the cost function shown in (8), which are obtained by substituting $\boldsymbol{u}_0$ and $\boldsymbol{u}_1$ into (8), respectively.

Finally, based on (9)–(12), the combined voltage vectors are figured out.

To simplify the predictive control, the voltage vector plane can be divided into six sectors, as illustrated in Figure 3. Then, according to the reference voltage shown in (6) and (7), its location can be obtained easily based on Table 1, where $\theta = \arctan(u_{\beta\text{ref}}/u_{\alpha\text{ref}})$.

Table 1. Sectors of the reference voltage.

Symbol	Angle Range	Sector
	$[0, 60°)$	I
	$[60°, 120°)$	II
θ	$[120°, 180°)$	III
	$[180°, 240°)$	IV
	$[240°, 300°)$	V
	$[300°, 360°)$	VI

Based on the position of the reference voltage, the alternative voltage vectors that should be evaluated online can be preselected based on Table 2. For instance, if the reference voltage is located at sector I, only $\boldsymbol{u}_{s1}$, $\boldsymbol{u}_{s2}$, and $\boldsymbol{u}_{s3}$ require to be evaluated online. So, as only three instead of twelve voltage vectors are required to be evaluated online, the calculation amount is reduced notably. Then, an optimal hybrid voltage vector among the three hybrid voltage vectors can be chosen to control the inverter in the next control cycle.

For clarity, Figure 4 is given to show the control principle of the presented strategy. Moreover, the detailed implementation steps are also depicted below.

Step 1: Calculate the reference voltage based on (6) and (7);

Step 2: Get the values of the reference voltage based on Table 1;

Step 3: Choose three candidate voltage vectors based on Table 2;

Step 4: Figure out the duty cycles of the basic voltage vectors that construct the three candidate voltage vectors based on (8) and (12);

Step 5: Get the values of the three candidate voltage vectors based on (9);

Step 6: Evaluate the cost function values of the three candidate voltage vectors based on (8) and select the voltage vector that can minimize the cost function as the optimal one.

Finally, the optimal vector is utilized to control the voltage source inverter.

Table 2. Voltage vector selection method.

Sector of the Reference Voltage	Selected Voltage Vectors
I	u_{s1}, u_{s2}, and u_{s3}
II	u_{s3}, u_{s4}, and u_{s5}
III	u_{s5}, u_{s6}, and u_{s7}
IV	u_{s7}, u_{s8}, and u_{s9}
V	u_{s9}, u_{s10}, and u_{s11}
VI	u_{s11}, u_{s12}, and u_{s1}
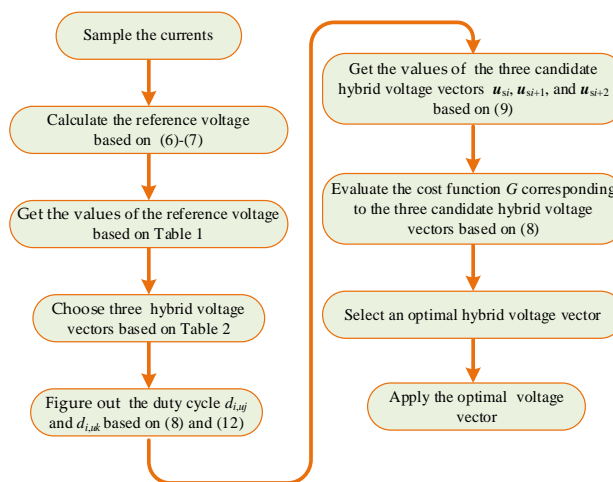
Figure 4. Control principle of the presented strategy.

4. Theoretical Analysis of the Proposed Method

To validate the correctness of the presented duty cycle calculation method shown in (11), a rigorous theoretical analysis is proposed. Here, the case that the reference voltage vector is located at sector I is taken as an example, where it overlaps with the segment OD in Figure 5.
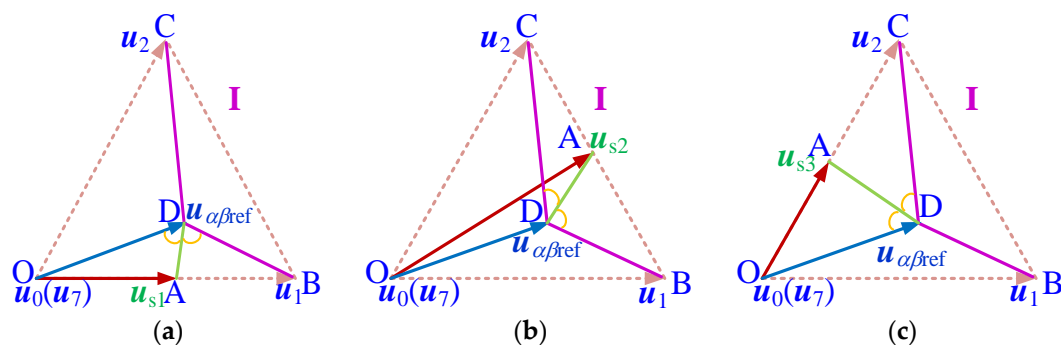
Figure 5. Schematic diagram of the effectiveness analysis. (**a**) Analysis of u_{s1}. (**b**) Analysis of u_{s2}. (**c**) Analysis of u_{s3}.

As u_{s1} is constructed by u_0 and u_1, their relationship has been shown in (10). Based on (10), (13) can be deduced.

$$\begin{aligned} u_{s1} &= u_0 + d_{1,u1}(u_1 - u_0) \\ &= u_1 + d_{1,u0}(u_0 - u_1) \end{aligned} \tag{13}$$

Based on (13) and Figure 5(a), it can be known that $|OA| = d_{1,u1}{}^*|u_1 - u_0|$ and $|AB| = d_{1,u0}{}^*|u_1 - u_0|$. Thus, $|OA|/|AB| = d_{1,u1}/d_{1,u0}$. According to (11) and (12), it can be deduced that

$$\frac{d_{1,u1}}{d_{1,u0}} = \frac{\sqrt{G_0}}{\sqrt{G_1}} \tag{14}$$

According to the cost function shown in (8), it can be known that

$$\begin{cases} G_0 = |OD|^2 \\ G_1 = |BD|^2 \end{cases} \tag{15}$$

Thus, it can be deduced that

$$\frac{|OA|}{|AB|} = \frac{|OD|}{|DB|} \tag{16}$$

By rearranging (16) with the law of sines in consideration, it can be further deduced that

$$\frac{\sin \angle ODA}{\sin \angle OAD} = \frac{|OA|}{|OD|} = \frac{|AB|}{|DB|} = \frac{\sin \angle ADB}{\sin \angle DAB} \tag{17}$$

Considering that $\angle OAD + \angle DAB = \pi$, it can be known that

$$\sin \angle OAD = \sin \angle DAB \tag{18}$$

Thus, (19) is finally deduced based on (17) and (18).

$$\sin \angle ODA = \sin \angle ADB \tag{19}$$

Based on (19), it can be calculated that $\angle ODA + \angle ADB = \pi$ or $\angle ODA = \angle ADB$. In the following, both of the two cases are analyzed respectively.

First, if $\angle ODA + \angle ADB = \pi$ is true, it can be calculated that point D must be located on the segment OB. In this situation, it can be figured out based on (16) that point D and point A will be the same point. That means $u_{s1} = u_{\alpha\beta ref}$ is true. Thus, the current control error can be minimized under this condition, which shows the validity of the duty cycle calculation algorithm proposed in this article.

Second, if point D is not located on the segment OB, $\angle ODA = \angle ADB$ should be true. In this situation, it can be obtained that $\angle ODA = \angle ADB < \angle OAD$ as $\angle OAD = \angle ADB + \angle DBA$. As $\angle DOA < \pi/3$ is true, and $\angle ODA + \angle OAD + \angle DOA = \pi$, it can be deduced that $\angle ODA + \angle OAD > 2\pi/3$. As $\angle OAD$ is larger than $\angle ODA$, $\angle OAD > \pi/3 > \angle ODA$ can be deduced. As $\angle DOA < \pi/3$ and $\angle OAD > \pi/3$ are true, it can be known that $\angle OAD > \angle DOA$. According to the law of sines, $|OD| > |AD|$ is finally deduced. As $|AD|$ stands for the square root value of the cost function of u_{s1}, and $|OD|$ denotes the square root value of the cost function of u_0, a conclusion is obtained, i.e., the control accuracy is increased when u_{s1} is utilized to replace u_0.

Similarly, it is easy to verify that $|DB| > |AD|$ is true, which means the control accuracy of u_{s1} is increased compared to that of u_1. Moreover, based on Figure 5b,c, it can also be verified that the control error can be reduced by using u_{s2} or u_{s3} instead of u_0, u_1, and u_2. This shows the validity of the proposed duty cycle calculation method in this work.

When the reference voltage vector locates at other sectors, similar results can be obtained. Therefore, the validity of the presented strategy is verified in terms of theory, which provides a solid foundation for its popularization and application.

5. Experimental Results

To further verify the correctness of the presented algorithm, an experimental prototype illustrated in Figure 6 is designed, including a two-level voltage source inverter, a DC power source, an AC power source, and a filter. Here, DSP28335 is selected as the controller, where the software code of the proposed algorithm is running in it. The experimental waveforms and data are recorded using an eight-channel oscilloscope. The parameters of the experimental system used in this work are listed in Table 3.
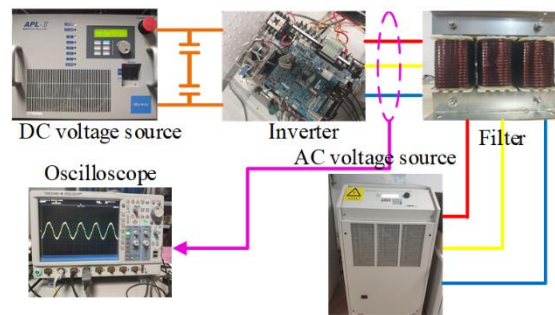
Figure 6. Photo of the experimental prototype.

Table 3. System parameters.

Symbol	Parameters	Values
u_{dc}	DC voltage	250 V
e	Peak of back EMF	150 V
L	Filter inductance	20 mH
R	Parasitic resistance	0.05 Ω
T	Sampling period	66.67 μs

5.1. Steady State Results

To verify the validity of the presented dual-vector modulated MPC algorithm for two-level source inverters, its steady state control performance is tested and compared with the conventional single-vector MPC.

In the first experiment, the reference current is set as 3 and 8 A, with the frequency of the back EMF set as 50 Hz. The results are depicted in Figures 7–10.
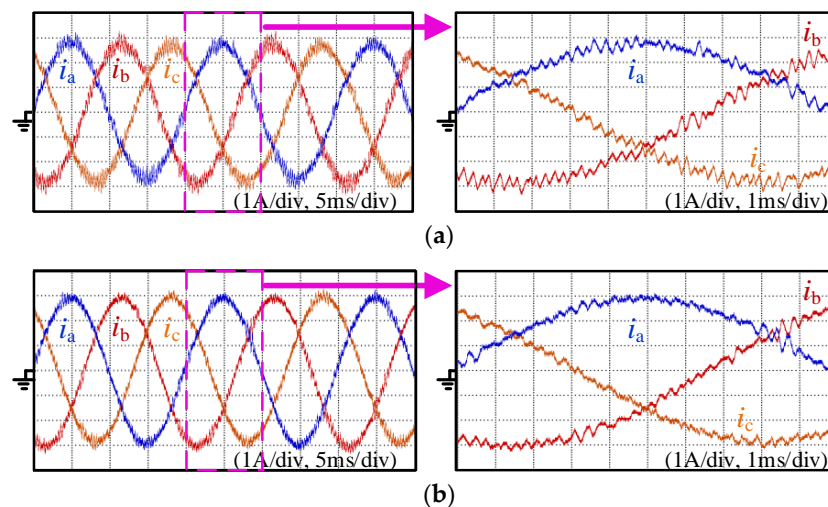

Figure 7. Current waveforms at 3 A. (**a**) The traditional model predictive control (MPC) method. (**b**) The presented MPC method.
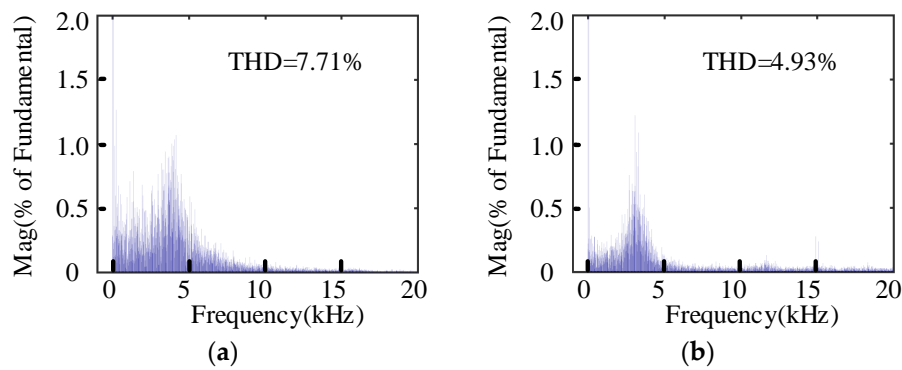
Figure 8. The current total harmonic distortion (THD) (3 A). (**a**) The traditional MPC strategy. (**b**) The presented MPC strategy.
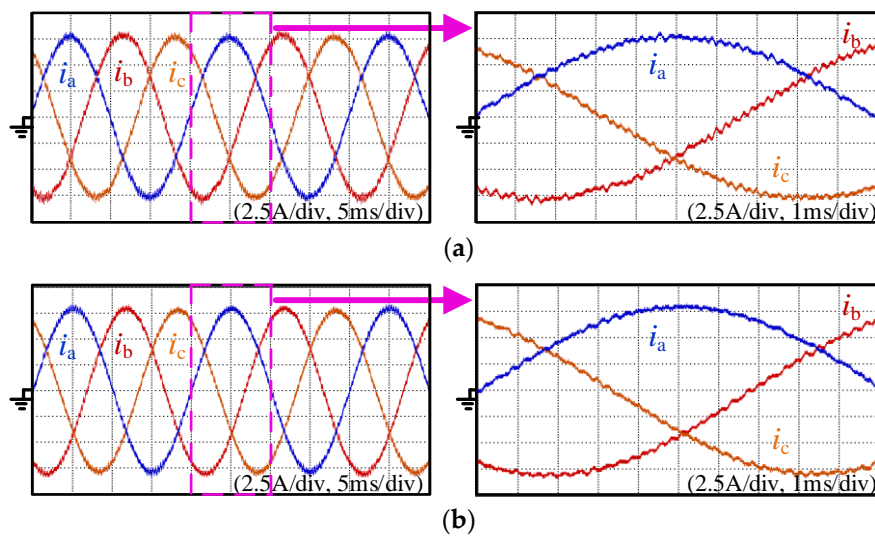

Figure 9. Current waveforms at 8 A. (**a**) The traditional MPC strategy. (**b**) The presented MPC strategy.
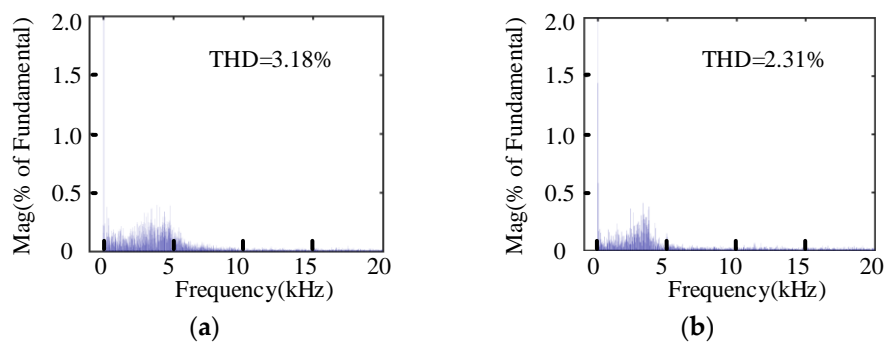

Figure 10. The current THD (8 A). (**a**) The traditional MPC strategy. (**b**) The presented MPC strategy.

Figure 7 illustrates the current waveforms when the reference current is set as 3 A. It is obvious to see that the current ripples of the conventional MPC method are larger than that of the proposed dual-vector modulated MPC strategy in this paper, which shows the validity of the presented method in this work.

Furthermore, Figure 8 shows the current THDs of the traditional MPC method as well as the proposed MPC method when the current is 3 A. It can be known from Figure 8 that the current THD is decreased obviously when the proposed MPC method instead of the traditional MPC method is utilized to control the two-level voltage source inverter, which shows the superiority of the proposed method again.

Additionally, Figure 9 depicts the current waveforms of the two methods when the current is set as 8 A with the current THDs depicted in Figure 10.

It is clear to see from Figure 9 that the current ripples of the presented MPC strategy are decreased compared to the conventional MPC method. Meanwhile, the current THDs of the presented method in this article are also reduced, as illustrated in Figure 10, which verifies the validity of the presented dual-vector modulated MPC strategy as well as the theoretical analysis again.

Furthermore, to show the superiority of the presented algorithm with different currents, another experiment is carried out, and the current THDs are recorded, plotted, and finally illustrated in Figure 11.
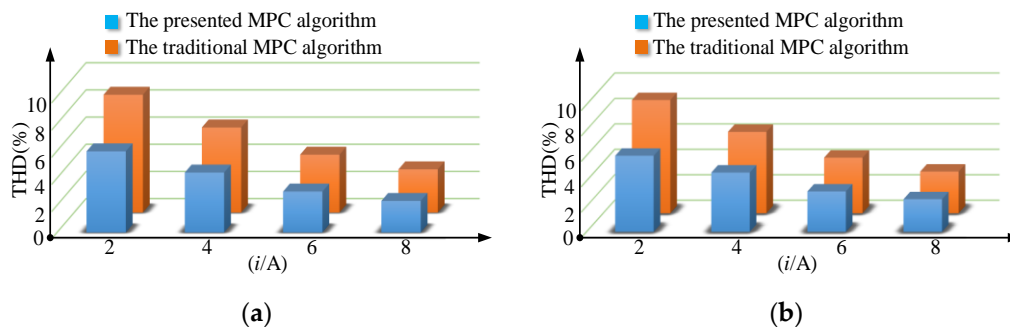

Figure 11. The current THDs with different currents. (**a**) The frequency is 50 Hz. (**b**) The frequency is 20 Hz.

Figure 11a shows the current THDs with different currents with the frequency set as 50 Hz. Figure 11b illustrates the current THDs with different currents at 20 Hz. It is apparent to see that the current THDs of the presented algorithm are decreased with different currents, which further verifies its validity.

5.2. Dynamic State Results

To further compare the dynamic state control performance of the presented algorithm with the conventional one, more experimental research is conducted here.

Figure 12a,b depicts the experimental waveforms of the double strategies when the current is stepped up from 3 to 8 A at 50 Hz. Figure 13a,b illustrates the results when the frequency is stepped up from 20 to 50 Hz with 8 A.
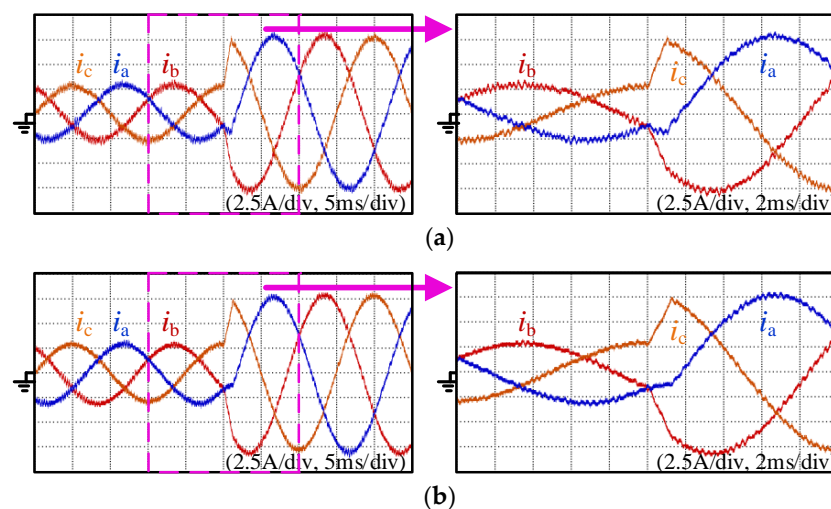

Figure 12. Dynamic current waveforms of the double strategies. (**a**) The traditional MPC strategy. (**b**) The presented MPC strategy.
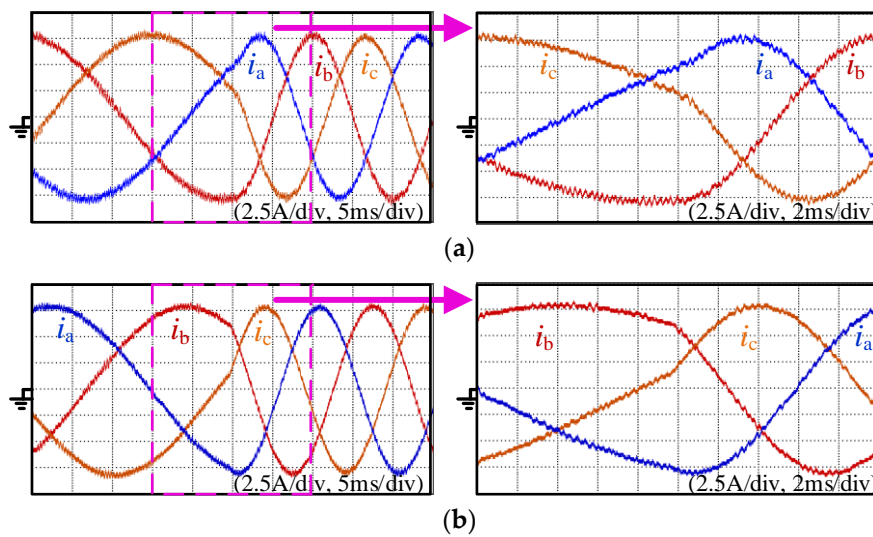
Figure 13. Dynamic current waveforms of the double strategies when the frequency changes. (**a**) The traditional MPC strategy. (**b**) The presented MPC strategy.

From Figures 12 and 13, it can be concluded that both of the double strategies can achieve a satisfactory dynamic control effect, which shows the effectiveness of the presented method when the current is changed suddenly. Besides, it is clear to see from Figures 12 and 13 that the current ripples of the presented dual-vector modulated MPC algorithm at steady state are lower than that of the conventional single-vector MPC method, which further verifies the effectiveness of the presented algorithm and the conducted theoretical analysis.

6. Extensions

Although the proposed dual-vector modulated MPC is aiming to control two-level voltage source inverters, further studies in this paper show that it can also be used to control other types of inverters by only changing the voltage vectors according to the corresponding inverter, which is another important contribution of this paper.

Here, a three-phase four-switch inverter is taken as an instance to show the correctness of the presented dual-vector modulated MPC.

Figure 14 shows the topology of the three-phase four-switch inverter. The four basic voltage vectors, i.e., V_1, V_2, V_3, and V_4, can be depicted as Figure 15, provided that the DC voltages are well balanced as many papers have studied the DC voltage balance control methods for three-phase four-switch inverters [33–36].
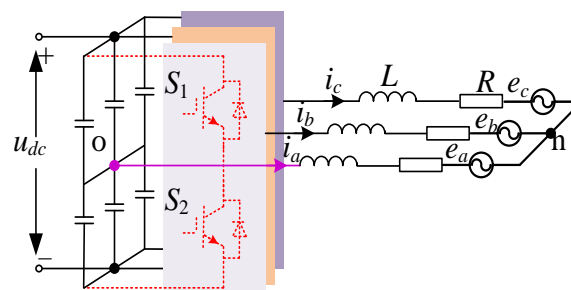

Figure 14. Topology of the three-phase four-switch inverter.

To reduce the current ripples, four hybrid voltage vectors are designed in the same way with (9), as shown in Figure 15, which are $V_{s1}(V_1, V_2)$, $V_{s2}(V_2, V_3)$, $V_{s3}(V_3, V_4)$, and $V_{s4}(V_4, V_1)$. In every control cycle, one of the four hybrid voltage vectors will be selected and utilized to reduce the current ripples.
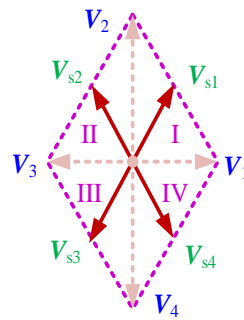
Figure 15. Voltage vectors of three-phase four-switch inverters.

The duty cycle of each voltage vector is calculated using the same method as (11). Then, after the four hybrid voltage vectors are determined, they are substituted into (8) to get an optimal one, which will then be utilized to control the three-phase four-switch inverter. The detailed implementation steps are similar to Figure 4. Furthermore, theoretical analysis and experimental studies are carried out to show its correctness and superiority.

6.1. Theoretical Analysis of the Proposed Method

For convenience, the voltage vector plane is divided into four sectors, as depicted in Figure 15. Here, the case that the reference voltage vector is located at sector I is taken as an example, as shown in Figure 16.
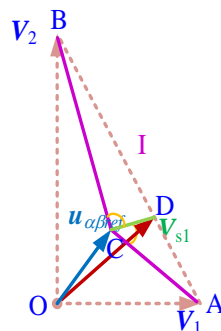

Figure 16. Schematic diagram for analyzing the correctness of the presented method for three-phase four-switch inverters.

First, it is assumed that the end point of V_{s1} is D, as shown in Figure 16.
Based on (9), (20) can be deduced.

$$V_{s1} = V_1 + d_{1,V2}(V_2 - V_1) \tag{20}$$

Thus, based on the geometrical relationship shown in Figure 16, (21) is deduced.

$$\begin{cases} |AD| = d_{1,V2}|(V_2 - V_1)| \\ |BD| = d_{1,V1}|(V_2 - V_1)| \end{cases} \tag{21}$$

Meanwhile, according to the duty cycle calculation method in (11), it can be deduced that

$$\frac{d_{1,V1}}{d_{1,V2}} = \frac{|BD|}{|AD|} = \frac{\sqrt{G_2}}{\sqrt{G_1}} \tag{22}$$

According the defined cost function in (8), it can be known that

$$\begin{cases} G_1 = |AC|^2 \\ G_2 = |BC|^2 \end{cases} \tag{23}$$

Thus, based on (22), it is calculated that

$$\frac{|BD|}{|AD|} = \frac{|BC|}{|AC|} \tag{24}$$

By rearranging (24) with the law of sines in consideration, (25) is obtained.

$$\frac{\sin \angle BCD}{\sin \angle BDC} = \frac{|BD|}{|BC|} = \frac{|AD|}{|AC|} = \frac{\sin \angle ACD}{\sin \angle ADC} \tag{25}$$

Considering that $\angle BDC + \angle ADC = \pi$, it can be known that

$$\sin \angle SDC = \sin \angle ADC \tag{26}$$

Thus, (27) is finally deduced based on (25) and (26).

$$\sin \angle BCD = \sin \angle ACD \tag{27}$$

Based on (27), it can be calculated that $\angle BCD + \angle ACD = \pi$ or $\angle BCD = \angle ACD$. In the following, both of the two cases are analyzed respectively.

First, if $\angle BCD + \angle ACD = \pi$ is true, it can be calculated that point C must be located on the segment AB. In this situation, it can be figured out based on (24) that point C and point D will be the same point. That means $V_{s1} = u_{\alpha\beta ref}$ is true. Thus, the current control error can be minimized under this condition, which shows the validity of the duty cycle calculation method proposed in this article.

Second, if point C is not located on the segment AB, $\angle BCD = \angle ACD$ should be true. In this situation, it can be obtained that $\angle BCD = \angle ACD < \angle ADC$ as $\angle ADC = \angle BCD + \angle CBD$. As $\angle CAD < \pi/3$ is true, and $\angle CAD + \angle ADC + \angle ACD = \pi$, it is obtained that $\angle ADC + \angle ACD > 2\pi/3$. As $\angle ADC$ is larger than $\angle ACD$, $\angle ADC > \pi/3 > \angle ACD$ can be obtained. As $\angle CAD < \pi/3$ and $\angle ADC > \pi/3$ are true, it can be known that $\angle ADC > \angle CAD$. Based on the law of sines, $|AC| > |CD|$ is finally deduced. Since $|AC|$ stands for the square root value of the cost function of V_1, and $|CD|$ denotes that of V_{s1}, a conclusion is obtained, i.e., the control accuracy is increased when V_{s1} is utilized to replace V_1.

Similarly, $|BC| > |CD|$ can be proved, which means the control accuracy of V_{s1} is increased compared to that of V_2. Thus, a conclusion is obtained, i.e., the proposed method is still effective when it is used to control the three-phase four-switch inverter. That is to say that the proposed method can be extended.

6.2. Experimental Verification

To validate the validity of the presented algorithm and the theoretical analysis shown above, experimental research is conducted, too. The parameters are the same as Table 3.

Figure 17 shows the current waveforms of the conventional single-vector MPC when the current is 4 A, while Figure 18 is the current waveforms of the proposed dual-vector modulated MPC under the same conditions.

It is clear to see from Figures 17 and 18 that when the proposed dual-vector modulated MPC method is utilized instead of the conventional single-vector MPC method, the current THD is decreased by 51.3%, which verifies the correctness of the presented strategy and the theoretical analysis again.

Additionally, compared to the conventional deadbeat control theory-based dual-vector MPC method [13–21], the proposed method in this paper can reduce the computational time, mainly because the duty cycle calculation method of this paper is simpler with reduced mathematical operation than

that of the conventional dual-vector MPC method [13–21]. Thus, less digital processing time is required. Furthermore, by using the proposed voltage-based cost function as well as the proposed voltage vector selection method in this paper, the computational time of the proposed method can be further reduced.
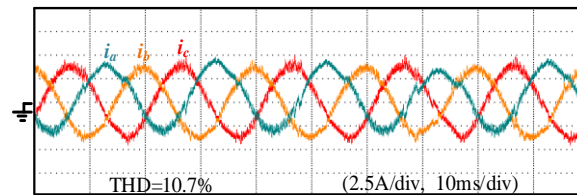

Figure 17. Current waveforms of the conventional single-vector MPC for the three-phase four-switch inverter.
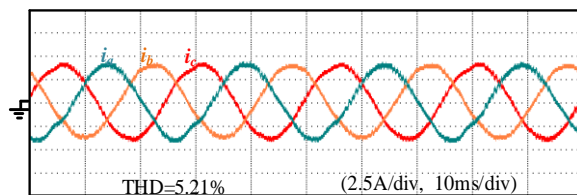

Figure 18. Current waveforms of the proposed dual-vector modulated MPC for the three-phase four-switch inverter.

7. Conclusions

In this paper, a dual-vector modulated MPC is proposed based on the hypothesis that the duty cycle of each voltage vector is inversely proportional to the square root of its corresponding cost function value for two-level voltage source inverters. Theoretical analysis is conducted based on the geometrical relationship of the voltage vectors for the first time to prove the correctness of the presented method. Furthermore, comparative experimental results show the superiority of the presented modulated MPC strategy, too. Moreover, at the end of the paper, the proposed dual-vector modulated MPC is extended to control the three-phase four-switch inverter. Both the theoretical analysis and the experimental results verify its effectiveness. This is another important contribution of this paper.

In the future, the proposed method should be further studied to control many other kinds of inverters, including multilevel inverters and matrix inverters, as they have similar voltage vector planes, and research should also be done to analyze its effectiveness in a similar way.

Nevertheless, the proposed method also has a few disadvantages, one of which being that although it can reduce the current ripples and THDs compared to the single-vector MPC, it cannot minimize the current ripples and THDs at all operation regions. Although the theoretical analysis shows that the proposed method can reduce the control error at all operation regions and minimize it in several special operation regions, no evidence shows that it can minimize the control error at all operation regions. Therefore, to further solve the disadvantages of the proposed method shown above and improve its control performance, much work should be done in the future to minimize the control error of the proposed method at all operation regions.

Author Contributions: L.C. and Y.L. proposed the main idea and contributed to the theoretical analysis of the proposed method. X.L. and L.G. contributed to the experiment study. N.J. and H.G. contributed to the experimental waveforms and data analysis. All authors have contributed to the writing of the paper. All authors have read and agreed to the published version of the manuscript.

Conflicts of Interest: The authors declare no conflict of interest.

References

1. Muhammad, A.A.; Ghulam, A.; Irfan, K.; Awan, A.B.; Farooq, U.; Saleem Khan, S.; Majeed, R. An impedance network-based three level quasi neutral point clamped inverter with high voltage Gain. *Energies* **2020**, *13*, 1261.
2. Adyr, A.E.; Alfredo, A.; Juvenal, R. Transformerless multilevel voltage-source inverter topology comparative study for PV systems. *Energies* **2020**, *13*, 3261.
3. Panos, C.P.; Konstantinos, F.K.; Antonio, T.A. Validation of novel PLL-driven PI control schemes on supporting VSIs in weak AC-connections. *Energies* **2020**, *13*, 1373.
4. Guo, L.; Jin, N.; Li, Y.; Luo, K. A model predictive control method for grid-connected power converters without AC voltage sensors. *IEEE Trans. Ind. Electron.* **2020**. Early Access. [CrossRef]
5. Zhang, X.; Gao, Q.; Hu, Y.; Zhang, H.; Guo, Z. Active power reserve photovoltaic virtual synchronization control technology. *Chin. J. Electr. Eng.* **2020**, *6*, 1–6. [CrossRef]
6. Rodriguez, J.; Pontt, J.; Silva, C.A.; Correa, P.; Lezana, P.; Cortés, P.; Ammann, U. Predictive current control of a voltage source inverter. *IEEE Trans. Ind. Electron.* **2007**, *54*, 495–503. [CrossRef]
7. Xia, C.; Liu, T.; Shi, T.; Song, Z. A simplified finite-control-set model-predictive control for power converters. *IEEE Trans. Ind. Inf.* **2014**, *10*, 991–1002.
8. Siami, M.; Arab Khaburi, D.; Rodriguez, J. Simplified finite control set-model predictive control for matrix converter-fed PMSM drives. *IEEE Trans. Power Electron.* **2018**, *33*, 2438–2446. [CrossRef]
9. Geyer, T.; Quevedo, D.E. Performance of multistep finite control set model predictive control for power electronics. *IEEE Trans. Power Electron.* **2015**, *30*, 1633–1644. [CrossRef]
10. Geyer, T.; Quevedo, D.E. Multistep finite control set model predictive control for power electronics. *IEEE Trans. Power Electron.* **2014**, *29*, 6836–6846. [CrossRef]
11. Guo, L.; Jin, N.; Gan, C.; Xu, L.; Wang, Q. An improved model predictive control strategy to reduce common-mode voltage for two-level voltage source inverters considering dead-time effects. *IEEE Trans. Ind. Electron.* **2019**, *66*, 3561–3572. [CrossRef]
12. Guo, L.; Jin, N.; Gan, C.; Luo, K. Hybrid voltage vector preselection based model predictive control for two-level voltage source inverters to reduce the common-mode voltage. *IEEE Trans. Ind. Electron.* **2020**, *67*, 4680–4691. [CrossRef]
13. Chen, W.; Zeng, S.; Zhang, G.; Shi, T.; Xia, C. A modified double vectors model predictive torque control of permanent magnet synchronous motor. *IEEE Trans. Power Electron.* **2019**, *34*, 11419–11428. [CrossRef]
14. Zhang, Y.; Xie, W.; Li, Z.; Zhang, Y. Low-complexity model predictive power control: Double-vector-based approach. *IEEE Trans. Ind. Electron.* **2014**, *61*, 5871–5880. [CrossRef]
15. Zhang, X.; Hou, B. Double vectors model predictive torque control without weighting factor based on voltage tracking error. *IEEE Trans. Power Electron.* **2018**, *33*, 2368–2380. [CrossRef]
16. Wang, X.; Sun, D. Three-vector-based low-complexity model predictive direct power control strategy for doubly fed induction generators. *IEEE Trans. Power Electron.* **2017**, *32*, 773–782. [CrossRef]
17. Kang, S.; Soh, J.; Kim, R. Symmetrical three-vector-based model predictive control with deadbeat solution for IPMSM in rotating reference frame. *IEEE Trans. Ind. Electron.* **2020**, *67*, 159–168. [CrossRef]
18. Guo, X.; Ren, H.; Li, J. Robust model-predictive control for a compound active-clamp three-phase soft-switching PFC converter under unbalanced grid condition. *IEEE Trans. Ind. Electron.* **2018**, *65*, 2156–2166. [CrossRef]
19. Zhou, D.; Li, X.; Tang, Y. Multiple-vector model-predictive power control of three-phase four-switch rectifiers with capacitor voltage balancing. *IEEE Trans. Power Electron.* **2018**, *33*, 5824–5835. [CrossRef]
20. Zhou, D.; Tu, P.; Tang, Y. Multivector model predictive power control of three-phase rectifiers with reduced power ripples under nonideal grid conditions. *IEEE Trans. Ind. Electron.* **2018**, *65*, 6850–6859. [CrossRef]
21. Zhang, Z.; Fang, H.; Gao, F.; Rodríguez, J.; Kennel, R. Multiple-vector model predictive power control for grid-tied wind turbine system with enhanced steady-state control performance. *IEEE Trans. Ind. Electron.* **2017**, *64*, 6287–6298. [CrossRef]
22. Tarisciotti, L.; Zanchetta, P.; Watson, A. Modulated model predictive control for a seven-level cascaded H-bridge back-to-back converter. *IEEE Trans. Ind. Electron.* **2014**, *61*, 5375–5383. [CrossRef]
23. Tarisciotti, L.; Zanchetta, P.; Watson, A.; Wheeler, P.; Clare, J.C.; Bifaretti, S. Multiobjective modulated model predictive control for a multilevel solid-state transformer. *IEEE Trans. Ind. Appl.* **2015**, *51*, 4051–4060. [CrossRef]

24. Vijayagopal, M.; Zanchetta, P.; Empringham, L.; De Lillo, L.; Tarisciotti, L.; Wheeler, P. Control of a direct matrix converter with modulated model-predictive control. *IEEE Trans. Ind. Appl.* **2017**, *53*, 2342–2349. [CrossRef]

25. Tarisciotti, L.; Lei, J.; Formentini, A.; Trentin, A.; Zanchetta, P.; Wheeler, P.; Rivera, M. Modulated predictive control for indirect matrix converter. *IEEE Trans. Ind. Appl.* **2017**, *53*, 4644–4654. [CrossRef]

26. Tarisciotti, L.; Formentini, A.; Gaeta, A.; Degano, M.; Zanchetta, P.; Rabbeni, R.; Pucci, M. Model predictive control for shunt active filters with fixed switching frequency. *IEEE Trans. Ind. Appl.* **2017**, *53*, 296–304. [CrossRef]

27. Li, X.; Peng, T.; Dan, H.; Zhang, G.; Tang, W.; Wheeler, P. A modulated model predictive control scheme for the brushless doubly fed induction machine. *IEEE J. Emerg. Sel. Top. Power Electron.* **2018**, *6*, 1681–1691. [CrossRef]

28. Yang, Y.; Wen, H.; Li, D. A fast and fixed switching frequency model predictive control with delay compensation for three-phase inverters. *IEEE Access* **2017**, *5*, 17904–17913. [CrossRef]

29. Guo, L.; Jin, Y.; Cao, L.; Dai, L.; Luo, K. Hybrid single and double-voltage vector-based model predictive common-mode voltage reduction method for 2-level voltage source inverters. *IET Power Electron.* **2019**, *12*, 2086–2094. [CrossRef]

30. Yang, H.; Zhang, Y.; Liu, J. Frequency-adaptive virtual flux estimator-based predictive power control with suppression of dc voltage ripples under unbalanced network. *IEEE Trans. Ind. Electron.* **2020**, *67*, 8969–8979. [CrossRef]

31. Scoltock, J.; Geyer, T.; Madawala, U.K. Model predictive direct power control for grid-connected NPC converters. *IEEE Trans. Ind. Electron.* **2015**, *62*, 5319–5328. [CrossRef]

32. CortÉs, P.; RodrÍguez, J.; Antoniewicz, P.; Kazmierkowski, M. Direct power control of an AFE using predictive control. *IEEE Trans. Power. Electron.* **2008**, *23*, 2516–2523. [CrossRef]

33. Sun, D.; Su, J.; Sun, C.; Nian, H. A simplified MPFC with capacitor voltage offset suppression for the four-switch three-phase inverter-fed PMSM drive. *IEEE Trans. Ind. Electron.* **2019**, *66*, 7633–7642. [CrossRef]

34. Zeng, Z.; Zhu, C.; Jin, X.; Shi, W.; Zhao, R. Hybrid space vector modulation strategy for torque ripple minimization in three-phase four-switch inverter-fed PMSM drives. *IEEE Trans. Ind. Electron.* **2017**, *64*, 2122–2134. [CrossRef]

35. Zhou, D.; Zhao, J.; Liu, Y. Predictive torque control scheme for three-phase four-switch inverter-fed induction motor drives with DC-link voltages offset suppression. *IEEE Trans. Power Electron.* **2015**, *30*, 3309–3318. [CrossRef]

36. Yuan, Q.; Zhao, R. DC-link capacitor voltage offset suppression with no filters for three-phase four-switch inverter fed PMSM drives. *Electron. Lett.* **2017**, *53*, 746–748. [CrossRef]